

# Weighted quantization using MMD: From mean field to mean shift via gradient flows

Ayoub Belhadji\*, Daniel Sharp\*, Youssef Marzouk

Center for Computational Science and Engineering  
Massachusetts Institute of Technology

February 18, 2025

## Abstract

Approximating a probability distribution using a set of particles is a fundamental problem in machine learning and statistics, with applications including clustering and quantization. Formally, we seek a finite weighted mixture of Dirac measures that best approximates the target distribution. While much existing work relies on the Wasserstein distance to quantify approximation errors, maximum mean discrepancy (MMD) has received comparatively less attention, especially when allowing for variable particle weights. We study the quantization problem from the perspective of minimizing MMD via gradient flow in the Wasserstein–Fisher–Rao (WFR) geometry. This gradient flow yields an ODE system from which we further derive a fixed-point algorithm called *mean shift interacting particles* (MSIP). We show that MSIP extends the (non-interacting) mean shift algorithm, widely used for identifying modes in kernel density estimates. Moreover, we show that MSIP can be interpreted as preconditioned gradient descent, and that it acts as a relaxation of Lloyd’s algorithm for clustering. Our numerical experiments demonstrate that MSIP and the WFR ODEs outperform other algorithms for quantization of multi-modal and high-dimensional targets.

## 1 Introduction

Numerous problems arising in statistics and machine learning involve approximating a probability measure using a small set of points, a task usually referred to as quantization Graf and Luschgy (2000). Examples include clustering Lloyd (1982), numerical integration Robert et al. (1999); Bach (2017) and teacher-student training of neural networks Chizat et al. (2019); Arbel et al. (2019). Formally, the quantization problem consists of seeking an approximation to a probability measure  $\pi$  using a mixture of Diracs  $\sum_{i=1}^M w_i \delta_{y_i}$ , where the  $y_i$  are usually called nodes or centroids and the  $w_i$  are weights. These nodes and weights are generally chosen to minimize  $D(\pi, \sum_{i=1}^M w_i \delta_{y_i})$ , where  $D$  quantifies the discrepancy between measures. Lloyd’s algorithm is probably the most iconic example of quantization Lloyd (1982). This algorithm aims to solve the optimization problem where  $D$  is taken to be the 2-Wasserstein distance and the weights are constrained to the simplex.

In this work, we focus on the case where  $D$  is the maximum mean discrepancy (MMD), a statistical pseudo-distance between two measures defined as follows: given a measurable space  $\mathcal{X}$

---

\*Equal contributions. Author emails: abelhadj@mit.edu, dannys4@mit.edu, ymarz@mit.edu

and a reproducing kernel Hilbert space (RKHS)  $\mathcal{H}$ , the MMD between measures  $\mu$  and  $\nu$  is defined as

$$\text{MMD}(\mu, \nu) := \sup_{\|f\|_{\mathcal{H}} \leq 1} \left| \int_{\mathcal{X}} f(x) d\mu(x) - \int_{\mathcal{X}} f(x) d\nu(x) \right|.$$

Compared to Wasserstein distances, MMD offers significant computational advantages, avoiding complex optimization problems and enabling efficient computation through kernel evaluations. Additionally, MMD exhibits favorable statistical properties in high-dimensional domains that are crucial for numerical integration tasks Muandet et al. (2017); Weed and Bach (2019). Initially introduced as a tool of statistical analysis and hypothesis testing (Gretton et al., 2007, 2012), MMD has since found applications in diverse fields ranging from generative modeling (Dziugaite et al., 2015; Li et al., 2017) to optimal transport (Chewi et al., 2024; Peyré and Cuturi, 2019).

More precisely, we consider the problem of MMD minimization under a cardinality constraint, formulated as

$$\min_{\mu \in \mathcal{M}_M(\mathcal{X})} \text{MMD}(\pi, \mu), \tag{1}$$

where  $\mathcal{M}_M(\mathcal{X})$  consists of mixtures of  $M$  Diracs  $\sum_{i=1}^M w_i \delta_{y_i}$  with  $y_i \in \mathcal{X}$  and  $w_i \in \mathbb{R}$ . This minimization problem can be seen as a relaxation of classical optimal quantization, where the weights  $w_i$  are constrained to the simplex.

As the quantization problem seeks to minimize a discrepancy between the target distribution  $\pi$  and a finite set of particles, this work is naturally connected to the study of gradient flows. A gradient flow traces a path through the space of measures. In particular, it minimizes a given “energy” functional by following the local direction of steepest descent defined according to a chosen geometry. This framework is amenable to numerical implementation, which in practice boils down to a discretization of the equations governing the gradient flow, often yielding an interacting particle system. Despite growing interest in the practice and theory of gradient flows Jordan et al. (1998); Otto (2001); Kondratyev et al. (2016); Craig and Bertozzi (2016); Santambrogio (2017); Gallouët and Monsaingeon (2017); Carrillo et al. (2019); Arbel et al. (2019); Chewi et al. (2020); Salim et al. (2020); Glaser et al. (2021); Korba et al. (2021); Lu et al. (2023); Maurais and Marzouk (2024); Chewi et al. (2024); Zhu and Mielke (2024), existing work largely focuses on the mean-field limit where the number of particles grows to infinity, conflicting with the motivation for quantization.

For this reason, we study (1) from two complementary perspectives. The first aligns naturally with research on gradient flows Arbel et al. (2019); Gladin et al. (2024), where we argue that the Wasserstein–Fisher–Rao (WFR) geometry is more flexible than the Wasserstein geometry for MMD minimization. From the second perspective, we exploit a novel connection between MMD minimization and the mean shift algorithm to derive a new analog of Lloyd’s algorithm.

Our **main contributions** are then as follows:

- We *unify* views of gradient flows, quantization, and mode-seeking methods for MMD minimization using a finite set of weighted particles.
- We employ the *Wasserstein–Fisher–Rao* (WFR) geometry for MMD minimization, which offers useful flexibility by allowing for both transport and the creation/destruction of mass. We represent the associated gradient flow with a mean-field ODE system that is efficient to solve using modern computational tools.
- We derive a new fixed-point iteration, named *mean shift interacting particles* (MSIP), that *directly* targets the steady-state solution of our WFR ODE. The weights of the proposed system naturally coincide with classical kernel-based quadrature constructions.

- We show that MSIP shares analytical and numerical similarities with both Lloyd’s algorithm for clustering and the mean shift algorithm for mode-seeking. We prove that the particle system is a *preconditioned gradient descent* of the function

$$(y_1, \dots, y_M) \mapsto \min_{w_i \in \mathbb{R}} \text{MMD} \left( \pi, \sum_{i=1}^M w_i \delta_{y_i} \right)^2.$$

- We demonstrate the computational *efficiency* and *robustness* of the proposed approaches for high-dimensional quantization problems, improving on current state-of-the-art methods. In particular, both MSIP and the WFR ODE yield *near-optimal* quantizations under MMD, even with extremely adversarial initializations.

This article is structured as follows. In Section 2, we review the literature on quantization, numerical integration in reproducing kernel Hilbert spaces (RKHS), the mean shift algorithm, and gradient flows. In Section 3 we present the main contributions of this work. In Section 4, we report on numerical experiments that illustrate the proposed algorithms. A short discussion concludes the article in Section 5.

**Notation** We denote by  $\mathcal{X}$  a subset of  $\mathbb{R}^d$ , and we use  $\mathcal{M}(\mathcal{X})$  and  $\mathcal{P}(\mathcal{X})$  to refer to the set of measures and probability measures supported on  $\mathcal{X}$ , respectively. Moreover, given  $M \in \mathbb{N}^*$ , we denote by  $\mathcal{X}^M$  the  $M$ -fold Cartesian product of  $\mathcal{X}$ , and by  $\mathcal{X}_{\neq}^M \subset \mathcal{X}^M$  the set

$$\mathcal{X}_{\neq}^M := \{(x_1, \dots, x_M) \in \mathcal{X}^M, \forall i \neq j \implies x_i \neq x_j\}.$$

We consider  $Y \in \mathcal{X}^M$  as a configuration of  $M$  points  $y_1, \dots, y_M \in \mathcal{X}$ . Since  $\mathcal{X} \subset \mathbb{R}^d$ , we abuse notation and let  $Y$  refer to the  $M \times d$  matrix whose rows are the vectors  $y_1, \dots, y_M$ . We also denote by  $\Delta_{M-1}$  the simplex of dimension  $M - 1$  defined by  $\{\mathbf{w} \in [0, 1]^M \mid \sum_{i \in [M]} w_i = 1\}$ . Consider  $\kappa : \mathcal{X} \times \mathcal{X} \rightarrow \mathbb{R}$  as the kernel associated to the RKHS  $\mathcal{H}$ . For a configuration  $Y$ , we denote by  $\mathbf{K}(Y) := (\kappa(y_i, y_j))_{i, j \in [M]}$  the associated kernel matrix for  $i, j \in [M]$ . Additionally, for a given real-valued function  $f : \mathcal{X} \rightarrow \mathbb{R}$ , we denote by  $\mathbf{f}(Y) := (f(y_i))_{i \in [M]}$  the vector of evaluations of  $f$  on the elements of  $Y$ . Finally, for a given vector-valued function  $\mathbf{g} : \mathcal{X} \rightarrow \mathbb{R}^d$ , we denote by  $\mathbf{g}(Y)$  the  $M \times d$  matrix where each row is an evaluation of  $\mathbf{g}$  on each  $y_i$ .

## 2 Background and Related Work

### 2.1 Numerical integration and quantization in RKHS

As it is at the core of many tasks in statistics and probability, we first review numerical methods to approximate integrals with a weighted sum of function evaluations at selected points Robert et al. (1999). Formally, for a measure  $\pi \in \mathcal{P}(\mathcal{X})$  and a function  $f : \mathcal{X} \rightarrow \mathbb{R}$ , a quadrature rule seeks to approximate  $\int_{\mathcal{X}} f(x) d\pi(x)$  with  $\sum_{i=1}^M w_i f(y_i)$ , where the points  $y_i \in \mathcal{X}$  are the quadrature nodes and the scalars  $w_i$  are the quadrature weights. To design a quadrature rule, we select representative nodes and weights to approximate the distribution  $\pi$ , essentially reducing the task to a quantization problem. Indeed, when the function  $f$  belongs to the RKHS  $\mathcal{H}$ , the integration error  $|\int_{\mathcal{X}} f(x) d\pi(x) - \sum_{i=1}^M w_i f(y_i)|$  is bounded by Muandet et al. (2017)

$$\|f\|_{\mathcal{H}} \text{MMD} \left( \pi, \sum_{i=1}^M w_i \delta_{y_i} \right). \quad (2)$$

In other words, having an accurate quantization with respect to MMD leads to a highly accurate quadrature rule  $\sum_{i=1}^M w_i \delta_{y_i}$  for functions living in the RKHS. Within this framework, the design of the quadrature rule remains independent of the function  $f$ , which is particularly advantageous in scenarios where evaluating  $f$  is expensive.

The *optimal kernel-based quadrature* is a popular and well-studied family of quadrature rules: for a given configuration of nodes  $Y$ , the weights  $\hat{w}_1(Y), \dots, \hat{w}_M(Y)$  satisfy

$$\text{MMD} \left( \pi, \sum_{i=1}^M \hat{w}_i(Y) \delta_{y_i} \right) \leq \text{MMD} \left( \pi, \sum_{i=1}^M w_i \delta_{y_i} \right), \quad (3)$$

for any  $w_1, \dots, w_M \in \mathbb{R}$ . These optimal weights can be expressed as the entries of the vector

$$\hat{\mathbf{w}}(Y) = \mathbf{K}(Y)^{-1} \mathbf{v}_0(Y), \quad (4)$$

where  $v_0 : \mathcal{X} \rightarrow \mathbb{R}$  is the *kernel mean embedding* of the probability measure  $\pi$  defined by

$$v_0(y) := \int_{\mathcal{X}} \kappa(x, y) d\pi(x). \quad (5)$$

While the optimal weights  $\hat{\mathbf{w}}(Y)$  have an analytical formula for fixed configuration  $Y$ , the function  $Y \mapsto \text{MMD}^2 \left( \pi, \sum_{i=1}^M \hat{w}_i(Y) \delta_{y_i} \right)$  is daunting to minimize due to its non-convexity. Recent work on optimal configurations often propose approaches tailored to specific classical probability measures (Gaussian measure, uniform measure on the hypercube, ...) Karvonen and Särkkä (2018, 2019); Ehler et al. (2019). Although there are some methods designed to be universal, their numerical implementation is generally limited by difficulties in high-dimensional domains. Examples include ridge leverage score sampling Bach (2017), determinantal point processes and volume sampling Belhadji et al. (2019, 2020); Belhadji (2021), Fekete points Karvonen et al. (2021), randomly pivoted Cholesky Epperly and Moreno (2023), or greedy selection algorithms De M. (2003); De M. et al. (2005); Santin and Haasdonk (2016); Oettershagen (2017); Huszár and Duvenaud (2012); Briol et al. (2015); Lacoste-Julien et al. (2015).

The function (5) is only practically tractable for some kernels and probability measures. One such case is when  $\pi$  is an empirical measure. In this case, the quantization can be seen as a summarization of<sup>1</sup>  $\pi$ , notably relevant for Bayesian inference Owen (2017); Riabiz et al. (2022). In this regard, many approaches were proposed in the literature: recombination Hayakawa et al. (2022, 2023), kernel thinning Dwivedi and Mackey (2021, 2024) and approximate ridge leverage score sampling Chatalic et al. (2023). This line of work is largely concerned with convergence rates in  $M$ , but the proposed methods are often outperformed in practice by simple algorithms (e.g., greedy methods) for small  $M$ .

## 2.2 Clustering

Lloyd’s algorithm is a standard method for quantization Lloyd (1982), which aims to solve the problem

$$\min_{Y \in \mathcal{X}^M} \min_{\mathbf{w} \in \Delta_{M-1}} W_2^2 \left( \pi, \sum_{i=1}^M w_i \delta_{y_i} \right), \quad (6)$$

where  $W_2$  is the 2-Wasserstein distance Peyré and Cuturi (2019). The solution of (6) is naturally expressed in terms of *Voronoi tessellations* Du et al. (1999). The Voronoi tessellation of a configuration

---

<sup>1</sup>Note that in general, the atoms of  $\pi$  are not necessarily i.i.d. samples from a distribution.

$Y \in \mathcal{X}^M$  corresponds to the sets  $\mathcal{V}_1(Y), \dots, \mathcal{V}_M(Y)$  defined by

$$\mathcal{V}_i(Y) := \left\{ x \in \mathcal{X} \mid i = \arg \min_{m \in [M]} \|x - y_m\| \right\}. \quad (7)$$

Given a mixture of Diracs  $\sum_{i=1}^M w_i \delta_{y_i}$ , the optimal transport plan from  $\pi$  to  $\sum_{i=1}^M w_i \delta_{y_i}$  maps all mass in the region  $\mathcal{V}_i(Y)$  to the atom located at  $y_i$ , and the total transportation cost can be written as  $\sum_{i=1}^M \int_{\mathcal{V}_i(Y)} \|x - y_i\|^2 d\pi(x)$ . Lloyd's algorithm is a fixed-point iteration aiming to minimize this cost jointly over the configuration  $Y$  and the vector of weights  $\mathbf{w}$  constrained to  $\Delta_{M-1}$ . More precisely, let  $Y^{(t)}$  be an iterate of the algorithm and  $\Psi_{\text{Lloyd}} : \mathcal{X}^M \rightarrow \mathcal{X}^M$  be the *Voronoi barycentric map* defined by

$$\forall i \in [M], (\Psi_{\text{Lloyd}}(Y))_{i,:} := \frac{\int_{\mathcal{V}_i(Y)} x d\pi(x)}{\int_{\mathcal{V}_i(Y)} d\pi(x)}. \quad (8)$$

The algorithm then consists of taking the fixed-point iteration  $Y^{(t+1)} = \Psi_{\text{Lloyd}}(Y^{(t)})$ . When  $Y \notin \mathcal{X}_{\neq}^M$ , the configuration of points is degenerate, i.e., the Voronoi tessellation is not uniquely defined, making the evaluation of  $\Psi_{\text{Lloyd}}(Y)$  ambiguous. However,  $\Psi_{\text{Lloyd}}$  preserves nondegeneracy in the sense that, if  $Y \in \mathcal{X}_{\neq}^M$  then  $\Psi_{\text{Lloyd}}(Y) \in \mathcal{X}_{\neq}^M$ , ensuring that the fixed-point iteration is closed Emelianenko et al. (2008). Interestingly, the fixed points of  $\Psi_{\text{Lloyd}}$  are critical points of the function  $G_M$ , defined as (Du et al., 1999, Proposition 6.2.)

$$G_M : Y \mapsto \min_{\mathbf{w} \in \Delta_{M-1}} W_2^2\left(\pi, \sum_{i \in [M]} w_i \delta_{y_i}\right). \quad (9)$$

The authors prove that  $G_M$  is differentiable in  $Y$  with the gradient given by

$$\nabla G_M(Y) = \mathbf{D}(Y)(Y - \Psi_{\text{Lloyd}}(Y)), \quad (10)$$

where  $\mathbf{D}(Y) \in \mathbb{R}^{M \times M}$  is a diagonal matrix with  $(\mathbf{D}(Y))_{i,i} := \int_{\mathcal{V}_i(Y)} d\pi(x)$ . Hence, the fixed-point iteration can be rewritten as a preconditioned gradient descent

$$Y^{(t+1)} = Y^{(t)} - \mathbf{D}(Y^{(t)})^{-1} \nabla G_M(Y^{(t)}). \quad (11)$$

The theoretical analysis of Lloyd's algorithm has been the subject of extensive study Kieffer (1982); Wu (1992); Du et al. (1999, 2006); Emelianenko et al. (2008); Pagès and Yu (2016); Portales et al. (2024).

### 2.3 Mean Shift

Mean shift is a widely used algorithm for tasks such as clustering Fukunaga and Hostetler (1975); Carreira-Perpinán (2015) and image segmentation Comaniciu and Meer (2002). The algorithm is a non-parametric method for locating the mode of a kernel density estimator (KDE) defined by

$$\hat{f}_{\text{KDE}}(y) := \frac{1}{N} \sum_{\ell=1}^N \kappa(y, x_\ell) = v_0(y), \quad (12)$$

where  $v_0$  is defined by (5) taking  $\pi$  to be the empirical measure associated to the data points  $x_1, \dots, x_N \in \mathcal{X}$ . In this context, the kernel  $\kappa$  must satisfy the following condition.

**Assumption 2.1.** The kernel  $\kappa$  is differentiable, and there exists a symmetric kernel  $\bar{\kappa} : \mathcal{X} \times \mathcal{X} \rightarrow \mathbb{R}$  satisfying

$$\forall x, y \in \mathcal{X}, \quad \nabla_2 \kappa(x, y) = (x - y) \bar{\kappa}(x, y). \quad (13)$$

Under this assumption, a critical point  $y_\star$  of the KDE satisfies  $\sum_{\ell=1}^N (y_\star - x_\ell) \bar{\kappa}(x_\ell, y_\star) = 0$ , which implies

$$y_\star = \Psi_{\text{MS}}(y_\star) := \frac{\sum_{\ell=1}^N x_\ell \bar{\kappa}(x_\ell, y_\star)}{\sum_{\ell=1}^N \bar{\kappa}(x_\ell, y_\star)}. \quad (14)$$

The mean shift algorithm seeks the location of  $y_\star$  using a fixed-point iteration on the map  $\Psi_{\text{MS}}$ . The convergence of the algorithm was extensively investigated in Cheng (1995); Li et al. (2007); Carreira-Perpinan (2007); Ghassabeh (2013, 2015); Arias-Castro et al. (2016); Yamasaki and Tanaka (2019, 2024). Theorem 2.1 is satisfied by many distance-based kernels defined as  $\kappa(x, y) = \varphi(\|x - y\|)$  for some function  $\varphi: \mathbb{R}^+ \rightarrow \mathbb{R}^+$  that is continuously differentiable almost everywhere. This includes the Gaussian kernel, the inverse multiquadric kernel (IMQ) and Matérn kernels.

## 2.4 Gradient flow methods for MMD minimization

A gradient flow of a functional  $\mathcal{F}$  on the space of positive measures  $\mathcal{M}_+(\mathcal{X})$  is a trajectory  $\mu_t$  satisfying the partial differential equation (PDE)

$$\dot{\mu}_t = -\text{grad}_d \mathcal{F}[\mu_t], \quad (15)$$

where  $\text{grad}_d \mathcal{F}$  denotes the gradient of  $\mathcal{F}$  with respect to a metric  $d: \mathcal{M}_+(\mathcal{X}) \times \mathcal{M}_+(\mathcal{X}) \rightarrow \mathbb{R}$ ; see Otto (2001); Ambrosio et al. (2008) for details. In practice, the solution of (15) can be approximated using numerical schemes such as time-splitting (Jordan et al., 1998).

In the following, we review existing constructions of gradient flows for minimizing the MMD. We highlight how the choice of metric  $d$ , and thus the underlying geometry, differentiates these approaches for minimizing the functional

$$\mathcal{F}(\mu) := \frac{1}{2} \text{MMD}(\mu, \pi)^2. \quad (16)$$

When the metric<sup>2</sup>  $d$  corresponds to the MMD, the equation (15) simplifies to  $\dot{\mu}_t = \mu_t - \pi$ , whose solution is given by  $\mu_t = e^{-t} \mu_0 + (1 - e^{-t}) \pi$ , where  $\mu_0$  is the initial condition (Gladin et al., 2024, Theorem 3.4). This solution is not suitable for the quantization problem we consider, as  $\pi$  generally cannot be expressed as a mixture of  $M$  Diracs.

Arbel et al. (2019) studied the gradient flow of  $\mathcal{F}$  under the 2-Wasserstein ( $W_2$ ) geometry, corresponding to the solution of

$$\dot{\mu}_t = \text{div} \left( \mu_t \nabla \tilde{\mathcal{F}}[\mu_t] \right), \quad (17)$$

where  $\tilde{\mathcal{F}}[\mu]$  is the first variation of  $\mathcal{F}$  at  $\mu$  given by

$$\tilde{\mathcal{F}}[\mu](\cdot) = \int_{\mathcal{X}} \kappa(\cdot, x) d\mu(x) - \int_{\mathcal{X}} \kappa(\cdot, x) d\pi(x). \quad (18)$$

The authors propose various numerical solutions to (17) based on discretizations in time and space. In particular, they replace the measures  $\mu_t$  by empirical counterparts, yielding a system of interacting particles. Moreover, they derive conditions for the convergence of their numerical schemes, and study the importance of *noise injection* as a regularization method. However, the approaches deteriorate dramatically when initialized poorly, requiring a large number of particles to converge. Further, rigidly constraining particles to have uniform weights is problematic; this can be

---

<sup>2</sup>Not to be confused with when  $\mathcal{F}$  is the MMD.

seen for  $M = 1$  when comparing gradient descent on the MMD to mean shift, which we discuss in Section 3.2.

An alternative geometry called *spherical interaction-force transport* (IFT) is proposed and studied in Gladin et al. (2024); Zhu and Mielke (2024). Inheriting properties of both the  $W_2$  and MMD geometries, the IFT gradient flow satisfies

$$\dot{\mu}_t = \alpha \operatorname{div} \left( \mu_t \nabla \tilde{\mathcal{F}}[\mu_t] \right) - \beta(\mu_t - \pi), \quad (19)$$

where  $\alpha, \beta \in \mathbb{R}$  are positive. The authors prove that if  $\mu_t$  solves (19), then  $\mathcal{F}[\mu_t]$  decays exponentially with  $t$  (Gladin et al., 2024, Theorem 3.5). While this is a remarkable theoretical result, it only holds in the mean-field limit  $M \rightarrow +\infty$ . They discretize (19) using a system of weighted interacting particles; as we show in Section 4, many of these particles tend to drift far away from the modes of  $\pi$ , making the resulting quantization inefficient for, e.g., quadrature. Further, the proposed implementation is complicated by an inner  $M$ -dimensional constrained optimization problem at every iteration.

Finally, the Wasserstein-Fisher-Rao (WFR) geometry allows both mass transport and total mass variation. The PDE corresponding to the WFR metric is

$$\dot{\mu}_t = \alpha \operatorname{div}(\mu_t \nabla \tilde{\mathcal{F}}[\mu_t]) - \beta \tilde{\mathcal{F}}[\mu_t] \mu_t. \quad (20)$$

This corresponds to a gradient flow of the functional  $\mathcal{F}$ , extending the  $W_2$  distance to measures with different total masses, i.e., *unbalanced* optimal transport. See Kondratyev et al. (2016); Gallouët and Monsaingeon (2017); Chizat et al. (2018); Liero et al. (2018) for details about the WFR metric, its geometric properties, and the construction of WFR gradient flows. Additionally, (Lu et al., 2019, 2023; Yan et al., 2024) provide theoretical and numerical results for the minimization of a kernelized KL divergence using the WFR geometry.

Compared to (17), equation (20) introduces  $\tilde{\mathcal{F}}[\mu_t] \mu_t$  as a reaction term, which allows the total mass of  $\mu_t$  to change as a function of  $t$ . Unbalanced transport allows for this creation or destruction of mass, which might be helpful when mass conservation is not a natural assumption. Despite this formulation, the numerical scheme proposed by Gladin et al. (2024) to solve (20) artificially conserves mass by projecting the weights onto the simplex; this is inconsistent with the PDE’s theoretical properties.

### 3 Main results

Based on the elements reviewed in Section 2, we contribute quantization schemes tailored for small values of  $M$ . This section is structured as follows: In Section 3.1, we propose simulating the WFR gradient flow to minimize the MMD using a weighted mixture of  $M$  Diracs. In Section 3.2, we use a sufficient condition for the WFR gradient flow’s steady state to derive a fixed-point iteration. Moreover, we demonstrate that this iteration can be expressed as a preconditioned gradient descent for a function related to the MMD. Further, the iteration is a natural extension of the mean shift algorithm.

#### 3.1 Simulating the WFR gradient flow using ODEs

Without loss of generality on the time-scale, we consider (20) with a reaction speed  $\beta \equiv 1$ . We seek  $\mu_t$  as a mixture of  $M$  Diracs, i.e.,  $\mu_t = \sum_{i=1}^M w_i^{(t)} \delta_{y_i^{(t)}}$ , where  $y_1^{(t)}, \dots, y_M^{(t)} \in \mathcal{X}$  and  $w_1^{(t)}, \dots, w_M^{(t)} \in \mathbb{R}$ .

**Proposition 3.1.** *Define the system of differential equations*

$$\begin{aligned}\dot{y}_i^{(t)} &= -\alpha \nabla \tilde{\mathcal{F}}[\mu_t](y_i^{(t)}) = -\alpha \left( \sum_{m=1}^M w_i^{(t)} \nabla_2 \kappa(y_m^{(t)}, y_i^{(t)}) - \nabla v_0(y_i^{(t)}) \right) \\ \dot{w}_i^{(t)} &= -w_i^{(t)} \tilde{\mathcal{F}}[\mu_t](y_i^{(t)}) = -w_i^{(t)} \left( \sum_{m=1}^M w_i^{(t)} \kappa(y_m^{(t)}, y_i^{(t)}) - v_0(y_i^{(t)}) \right)\end{aligned}\tag{21}$$

where  $i \in [M]$ , and  $v_0$  as defined in (5). If the trajectory  $(\mu_t)_{t \geq 0}$  satisfies (21), then  $(\mu_t)_{t \geq 0}$  weakly satisfies (20).

The proof and a more detailed account of Theorem 3.1 are given in Appendix B.1. We can use standard ODE solvers to efficiently approximate  $\mu_t$  provided the function  $v_0$  can be evaluated. For instance, when  $\pi$  is an empirical measure of  $N$  atoms in  $\mathbb{R}^d$ , the system of equations (21) can be implemented in  $O(d(M+N)M)$  operations<sup>3</sup>.

Informally, if  $w_i^{(0)} > 0$ , we are ensured that  $w_i^{(t)} \geq 0$  for sufficiently small  $t$  by the structure of (21). To understand this, we consider the sign of the term  $\tilde{\mathcal{F}}[\mu_t](y_i^{(t)})$ : If this term is negative, then  $w_i^{(t)}$  will increase locally in  $t$ , drifting away from 0. However, if the term is positive, the weight  $w_i^{(t)}$  locally decreases toward a steady state  $w_i^{(t)} \equiv 0$ . This argument only holds for operator  $\tilde{\mathcal{F}}$  that is continuously differentiable in  $\mu_t$ .

### 3.2 A fixed-point scheme for steady-state solutions

While the solution to (21) is an entire trajectory  $(\mu_t)_{t \geq 0}$ , we are primarily interested in  $\mu_\infty$ ; if it exists, it should be a minimizer to the functional  $\mathcal{F}$ . To find  $\mu_\infty$ , we look for a steady state solution satisfying  $\dot{y}_i^{(t)} \equiv 0$  and  $\dot{w}_i^{(t)} \equiv 0$ , which is ensured by the sufficient condition for all  $i \in [M]$

$$\sum_{m=1}^M w_m \kappa(y_m, y_i) = \int_{\mathcal{X}} \kappa(x, y_i) d\pi(x)\tag{22}$$

$$\sum_{m=1}^M w_m \nabla_2 \kappa(y_m, y_i) = \int_{\mathcal{X}} \nabla_2 \kappa(x, y_i) d\pi(x).\tag{23}$$

The condition (22) is prevalent in the literature of kernel-based quadrature, and reflects that the quadrature rule defined by the measure  $\mu = \sum_{m=1}^M w_m \delta_{y_m}$  is exact on the subspace spanned by the functions  $\kappa(\cdot, y_i)$ . Note that equation (22) enforces optimal kernel quadrature weights  $\hat{\mathbf{w}}(Y) = \mathbf{K}(Y)^{-1} \mathbf{v}_0(Y)$ , as in (4), and the resulting quadrature rule thus satisfies the optimality property (3). Now, we explore the second condition (23), less known in the literature, when making Theorem 2.1.

**Proposition 3.2.** *Let  $Y \in \mathcal{X}^M$ . Under Theorem 2.1 and assuming that the gradient of  $\kappa$  is bounded on  $\mathcal{X}$ , the equations (22) and (23) imply that*

$$\bar{\mathbf{K}}(Y) \mathbf{W}(Y) Y = \bar{\mathbf{v}}_1(Y) + \bar{\mathbf{u}}(Y),\tag{24}$$

where  $\bar{\mathbf{K}}(Y) \in \mathbb{R}^{M \times M}$  is the kernel matrix with the kernel  $\bar{\kappa}$ , diagonal matrix  $\mathbf{W}(Y)$  has entries corresponding to those of  $\hat{\mathbf{w}}(Y)$  given by (4), and  $\bar{\mathbf{v}}_1(Y), \bar{\mathbf{u}}(Y) \in \mathbb{R}^{M \times d}$  are the matrices with rows

<sup>3</sup>This assumes that evaluating  $\kappa$  is  $O(1)$  and  $\nabla_2 \kappa$  is  $O(d)$ .

defined as

$$\begin{aligned} (\bar{\mathbf{v}}_1(Y))_{i,:} &:= \int_{\mathcal{X}} x \bar{\kappa}(x, y_i) \, d\pi(x), \\ (\bar{\mathbf{u}}(Y))_{i,:} &:= \left( \sum_{m=1}^M w_m \bar{\kappa}(y_m, y_i) - \int_{\mathcal{X}} \bar{\kappa}(x, y_i) \, d\pi(x) \right) y_i. \end{aligned} \quad (25)$$

The equation (24) does not admit a tractable closed-form solution for  $Y$ . We propose a sequence  $(Y^{(t)})_t$  satisfying

$$\bar{\mathbf{K}}(Y^{(t)}) \mathbf{W}(Y^{(t)}) Y^{(t+1)} = \hat{\mathbf{v}}_1(Y^{(t)}), \quad (26)$$

where

$$\hat{\mathbf{v}}_1(Y) := \bar{\mathbf{v}}_1(Y) + \bar{\mathbf{u}}(Y). \quad (27)$$

Under the assumption that the kernel matrices  $\mathbf{K}(Y^{(t)})$  and  $\bar{\mathbf{K}}(Y^{(t)})$  are non-singular, the relationship (26) is expressed as a fixed-point iteration  $Y^{(t+1)} = \Psi_{\text{MSIP}}(Y^{(t)})$ , where

$$\Psi_{\text{MSIP}}(Y) := \mathbf{W}(Y)^{-1} \bar{\mathbf{K}}(Y)^{-1} \hat{\mathbf{v}}_1(Y). \quad (28)$$

We call  $\Psi_{\text{MSIP}}$  the *mean shift interacting particles* map. When  $\kappa$  is the squared exponential kernel, there exists a scalar  $\lambda \in \mathbb{R}$  such that  $\bar{\kappa} = \lambda \kappa$ ; then, the condition (3) implies  $\bar{\mathbf{u}}(Y) = 0$ , and (28) simplifies to

$$Y^{(t+1)} = \mathbf{W}(Y^{(t)})^{-1} \mathbf{K}(Y^{(t)})^{-1} \mathbf{v}_1(Y^{(t)}), \quad (29)$$

where  $(\mathbf{v}_1(Y))_{i,:} := \int_{\mathcal{X}} x \kappa(y_i, x) \, d\pi(x)$ . The proof of Theorem 3.2 is given in Appendix B.2.

**Damped fixed-point iteration** In the following, we prove that the fixed-point algorithm defined using (28) can be seen as a preconditioned gradient descent iteration on the function  $F_M : \mathcal{X}_{\neq}^M \rightarrow \mathbb{R}$  given by

$$F_M(y_1, \dots, y_M) := \inf_{\mathbf{w} \in \mathbb{R}^M} \mathcal{F} \left[ \sum_{i=1}^M w_i \delta_{y_i} \right]. \quad (30)$$

We start with the following result.

**Theorem 3.3.** *Under Theorem 2.1, the gradient of  $F$ , seen as an  $M \times d$  matrix, is given by*

$$\begin{aligned} \nabla F_M(Y) &= \mathbf{W}(Y) (\bar{\mathbf{K}}(Y) \mathbf{W}(Y) Y - \hat{\mathbf{v}}_1(Y)) \\ &= \mathbf{W}(Y) \bar{\mathbf{K}}(Y) \mathbf{W}(Y) (Y - \Psi_{\text{MSIP}}(Y)), \end{aligned} \quad (31)$$

with  $\Psi_{\text{MSIP}}(Y)$  is defined in (28), where the latter equality holds when  $\mathbf{W}(Y) \bar{\mathbf{K}}(Y) \mathbf{W}(Y)$  is invertible. In particular, for the Gaussian kernel, the expression simplifies to

$$\nabla F_M(Y) = \mathbf{W}(Y) \mathbf{K}(Y) \mathbf{W}(Y) (Y - \Psi_{\text{MSIP}}(Y)).$$

The identity (31) proves that the fixed points of the function  $\Psi_{\text{MSIP}}$  are critical points of the function  $F_M$ . This result is reminiscent of (10) proved in Du et al. (1999), which gives a similar characterization of the fixed points of Lloyd's map  $\Psi_{\text{Lloyd}}$ . Following the same reasoning as in Portales et al. (2024), we deduce from (31) that the fixed point iteration defined by (28) is a

preconditioned gradient descent, with  $\mathbf{M}(Y) := \mathbf{W}(Y)\bar{\mathbf{K}}(Y)\mathbf{W}(Y)$  as the preconditioning matrix. Indeed, if the matrix  $\mathbf{M}(Y^{(t)})$  is non-singular, combining (28) and (31) yields

$$Y^{(t+1)} = Y^{(t)} - \mathbf{M}(Y^{(t)})^{-1} \nabla F_M(Y^{(t)}). \quad (32)$$

Now, if we choose a step size  $\eta$  for (32), we get

$$\begin{aligned} Y^{(t+1)} &= Y^{(t)} - \eta \mathbf{M}(Y^{(t)})^{-1} \nabla F_M(Y^{(t)}) \\ &= (1 - \eta)Y^{(t)} + \eta \Psi_{\text{MSIP}}(Y^{(t)}), \end{aligned} \quad (33)$$

which is equivalent to a damped fixed-point iteration on  $\Psi_{\text{MSIP}}$  Kelley (2018).

**Mean shift through the lens of MMD minimization** In the case  $M = 1$ , we see that the classical mean shift algorithm identifies critical points of the function  $F_1$ .

**Corollary 3.4.** *Under Theorem 2.1, we have*

$$\nabla F_1(y) = \frac{v_0(y)}{\kappa(y, y)} (\bar{v}_0(y)y - \bar{v}_1(y)), \quad (34)$$

where  $\bar{v}_0(y) := \int_{\mathcal{X}} \bar{\kappa}(x, y) d\pi(x) \in \mathbb{R}$ .

Thus, a critical point  $y$  of  $F_1$  is either a zero of  $v_0$  or satisfies

$$y = \frac{\bar{v}_1(y)}{\bar{v}_0(y)} = \frac{\int_{\mathcal{X}} x \bar{\kappa}(x, y) d\pi(x)}{\int_{\mathcal{X}} \bar{\kappa}(x, y) d\pi(x)}, \quad (35)$$

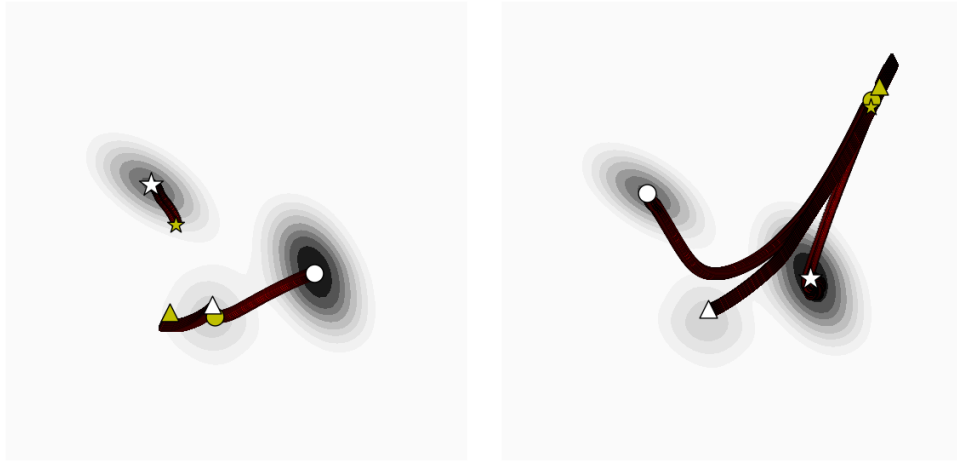
if the ratio is well-defined. In particular, when  $\pi$  is taken to be an empirical measure  $\pi = \frac{1}{N} \sum_{n=1}^N \delta_{x_n}$ , any point  $y^*$  that satisfies  $\Psi_{\text{MS}}(y^*) \equiv y^*$  as in (14) is a critical point of  $F_1$ . Then, the mean shift algorithm becomes a special case of the fixed-point iteration defined in Section 3.2 when  $M = 1$ . The proof of Theorem 3.4 is given in Appendix B.4 as a direct consequence of Theorem 3.3.

We now contrast (35) with an unweighted Wasserstein gradient flow for the MMD, as given in (Arbel et al., 2019), when  $M = 1$ . In particular, the path traced using the  $W_2$  geometry will use the gradient of the first variation given by  $\nabla \tilde{\mathcal{F}}(y) = y\bar{v}_0(y) - \bar{v}_1(y)$ . When  $y$  is far from the data, both  $\bar{v}_0(y)$  and  $\bar{v}_1(y)$  will vanish and thus the particle’s speed vanishes along with them. On the other hand, mean shift ameliorates this through the inverse operation in (35), magnifying the gradient considerably.

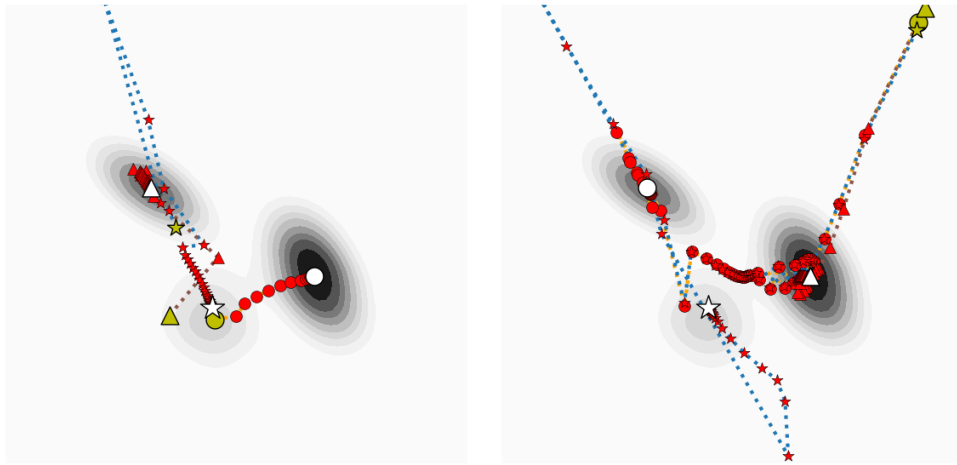
## 4 Numerical Results

In the following, we summarize the results of numerical simulations that validate the proposed algorithms. In Section 4.1 we conduct numerical experiments on synthetic Gaussian mixture datasets, while in Section 4.2, we perform the experiments on MNIST. All experiments<sup>4</sup> were performed in Python using the Numba library (Lam et al., 2015) using MIT SuperCloud resources (Reuther et al., 2018).

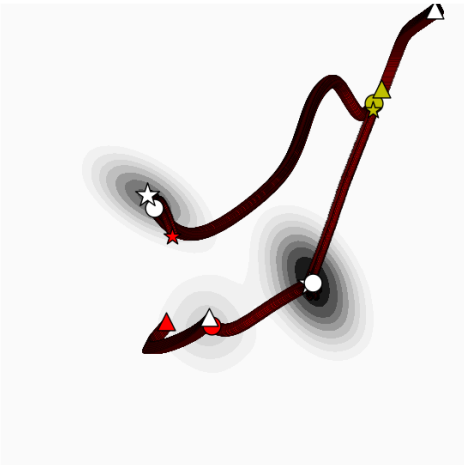
<sup>4</sup>Code used for experiments is freely available at [github.com/AyoubBelhadji/disruptive\\_quantization](https://github.com/AyoubBelhadji/disruptive_quantization)



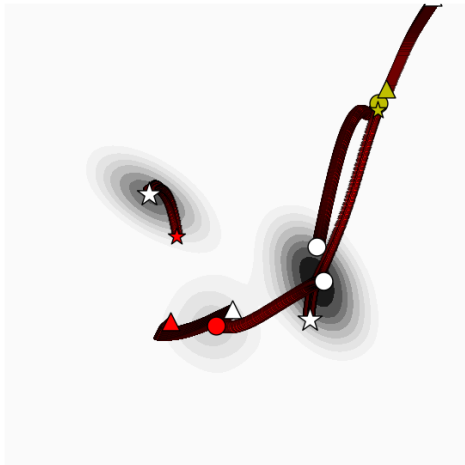
(a) WFR



(b) MSIP



(c) IFTFlow



(d) MMDGF

Figure 1: Trajectories of four algorithms started at two different initializations (yellow and red symbols). Each marker is one iteration for a particle, and the lines show particle paths. White markers are the final particle positions.

## 4.1 Experiment 1: a synthetic dataset

In this section, we compare various algorithms of MMD minimization on synthetic datasets, for which the construction is detailed in Appendix A.2.

We start with a qualitative comparison of the following algorithms: i) Wasserstein-Fisher-Rao Flow for MMD (WFR) introduced in Section 3.1, ii) mean shift interacting particles (MSIP) introduced in Section 3.2, iii) IFTflow introduced in Gladin et al. (2024), iv) MMD gradient flow (MMDGF) introduced in Arbel et al. (2019). Figure 1 compares the dynamics of the four algorithms for the first 1000 iterations. For WFR and MSIP, we display in separate plots the dynamics when matching three nodes to a mixture of three Gaussians with two different initializations: random elements of the dataset (left), and points far from the support of  $\pi$  (right). For each of IFTFlow and MMDGF, we demonstrate both scenarios in the same plot. The lines indicate particle trajectories, where markers overlapping indicate slower dynamics. In particular, we see WFR performing well in both scenarios with sufficient compute, where MSIP is significantly faster; while MSIP produces erratic trajectories and might overshoot the support, it converges at the end. In contrast, both MMDGF and IFTFlow succeed when starting from the support, but perform poorly otherwise.

When comparing the algorithms quantitatively, we evaluate six algorithms: i)  $k$ -means, ii) MMDGF, iii) IFTflow, iv) WFR, v) MSIP, vi) plain gradient descent on the function  $F_M$  defined by (30), which we refer to as discrepancy minimizing gradient descent (DMGD).

We present in Figure 2 the MMD as a function of the iteration for the measures obtained from running each algorithm on 100 initializations. For each algorithm iteration, we plot the highest and lowest MMD value across all 100 initializations. As a benchmark, we use the square root of the  $(M + 1)$ -st eigenvalue of the integration operator associated with the kernel  $\kappa$  and the probability measure  $\pi$ , divided by  $\|\mathbf{v}_0\|_{\mathcal{H}}$ . The eigenvalues of this operator are classically used in measuring the complexity of numerical integration in an RKHS; see Pinkus (2012); Bach (2017).

We observe that, even in the worst case for  $d = 2$ , MSIP consistently outperforms other quantization algorithms, where it quickly converges to a near-optimal quantization under the MMD. Similarly, WFR slowly descends in the MMD, surpassing  $k$ -means given enough iterations. In the best case, we see high performance from all the algorithms except for MMDGF. When  $d = 100$ , we have a more difficult approximation problem, where MSIP is still robust to initialization and WFR performs comparably to  $k$ -means in the worst case and MSIP in the best case. Other algorithms struggle in this high-dimensional problem.

## 4.2 Experience 2: MNIST

We now illustrate using the MNIST dataset qualitatively; for a quantitative results, see Appendix A.3.2. We compare MSIP, Lloyd’s algorithm, WFR, IFTflow, MMDGF, DMGD, and mean shift without interaction (IIDMS). More precisely, IIDMS refers to the mean shift algorithm without interactions initialized with i.i.d. samples. When using Lloyd’s algorithm with an empty Voronoi cell, we make the corresponding particle retain its position.

Figure 3 shows the results of 5000 iterations for each algorithm, all initialized with the same set of  $M$  i.i.d. samples drawn from the uniform distribution on the hypercube  $[0, 1]^{784}$ . We use a Matérn kernel with a bandwidth of  $\sigma = 2.25$  and smoothness of  $\nu = 1.5$ . We see that MSIP and WFR recover recognizable digits. If we examine the MSIP and WFR results, each output has two particles that look like ones: these image pairs correspond to different modes of MNIST with a separating distance larger than  $\sigma$ . While IIDMS converges to a mode, it lacks the diversity of MSIP. On the other hand, Lloyd’s algorithm has problems effectively using all centroids, as

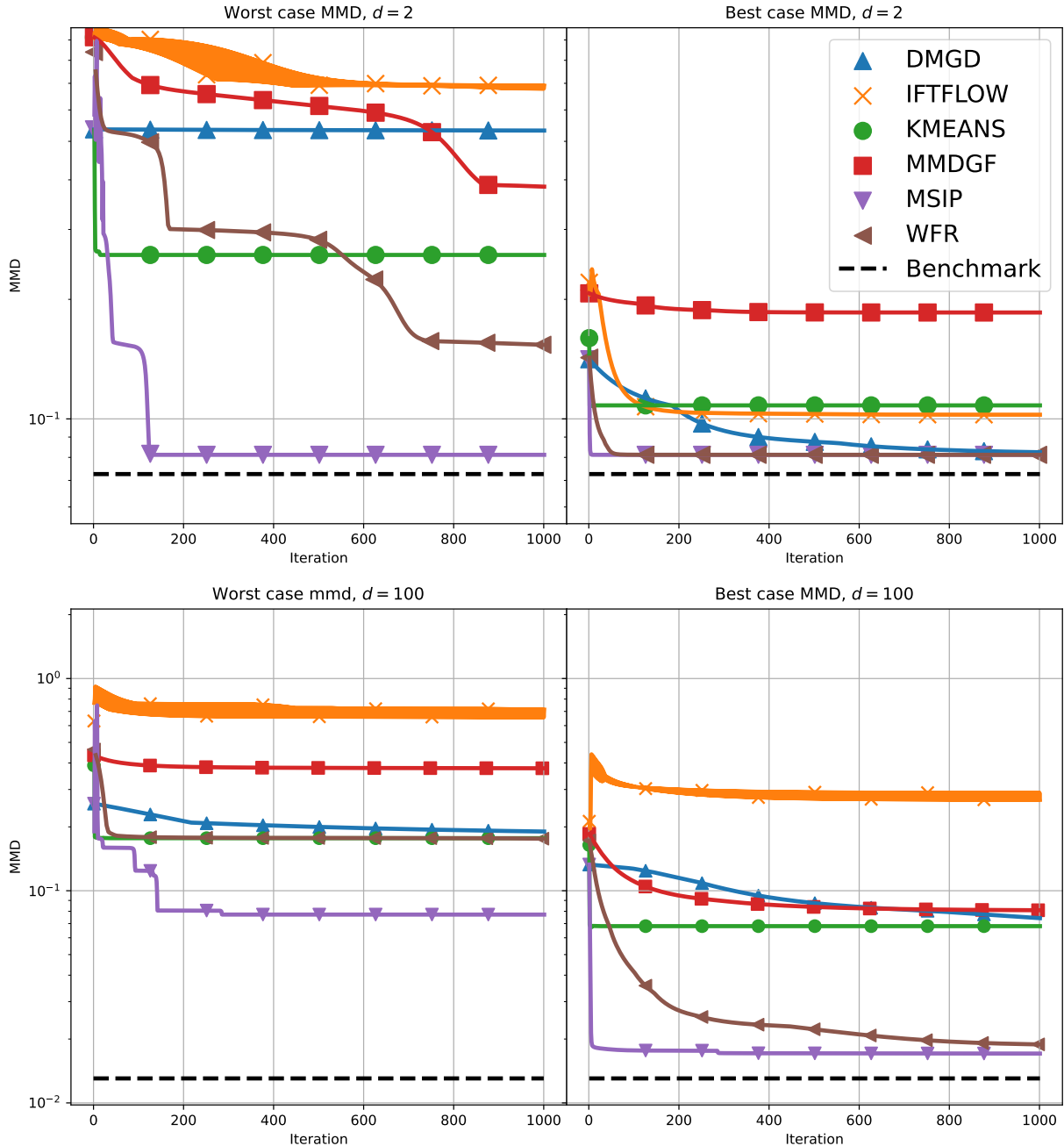


Figure 2: Comparison of different quantization algorithms on a GMM. (Top): dimension  $d = 2$ ,  $M_0 = M = 3$ . (Bottom): dimension  $d = 100$ ,  $M_0 = 5$ ,  $M = 10$ . We use bandwidth  $\sigma = 5$  for a squared-exponential kernel for all kernel-based algorithms and tried to provide hyperparameter tuning for each algorithm.

many particles have an empty Voronoi cell across all iterations<sup>5</sup>; remaining particles are extended between many digits. The other three algorithms remain trapped far from the distribution’s support. This experiment illustrates the capacity of the proposed algorithms to detect diverse modes for

<sup>5</sup>Lloyd’s algorithm is typically initialized from the data distribution itself to mitigate this phenomenon.

a multi-modal distribution. Our algorithms show remarkable robustness to initialization, even in high-dimensional domains.

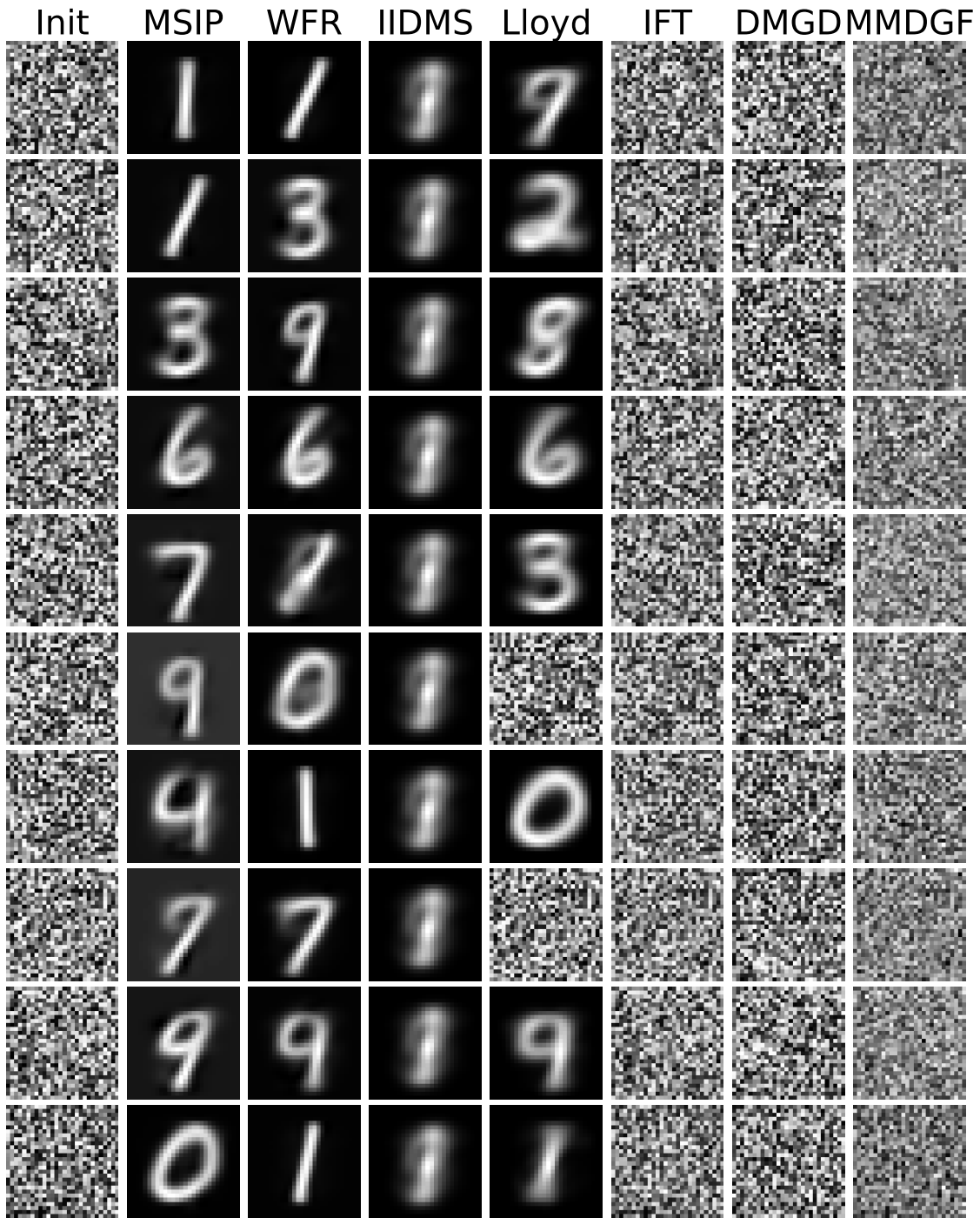


Figure 3: Comparison of different algorithms on MNIST.

## 5 Discussion

In light of the established similarities between MSIP and Lloyd’s algorithm, this work opens the door to further theoretical developments for MMD minimization which bypass mean-field analysis. In particular, Theorem 3.3 suggests that the extensive theory developed for Lloyd’s algorithm may be leveraged for MSIP. For instance, a natural question is whether this analogy extends further through an analysis of the non-degeneracy of the map  $\Psi_{\text{MSIP}}$  Emelianenko et al. (2008), which would allow us to prove that MSIP converges to critical points of the MMD. In this regard, a promising direction would be to study the monotonicity of the MMD for the iterates of MSIP, where Theorem 3.3 might be useful. For this, the rich literature on quasi-Newton methods could further our understanding of MSIP and WFR Nocedal and Wright (1999). Proving a descent property for MSIP would involve studying technical properties of the method, including analyzing second order properties of the function  $F_M$  as was done for Lloyd’s map Du et al. (1999). Beyond convergence guarantees, an interesting direction for future research is to explore the impact of this approach on the understanding of neural network training, as studied in Arbel et al. (2019); Rotskoff et al. (2019), and on sparse measure reconstructions De Castro and Gamboa (2012); Chizat (2022); Belhadji and Gribonval (2024). Generally, our methods show promising results for mode-seeking using interacting particle systems, which we hope will better tackle general non-convex high-dimensional approximation problems.

## 6 Acknowledgements

AB, DS, and YM acknowledge support from the US Department of Energy (DOE), Office of Advanced Scientific Computing Research, under grants DE-SC0021226 (FASTMath SciDAC Institute) and DE-SC0023188. AB and YM also acknowledge support from the ExxonMobil Technology and Engineering Company. The authors also acknowledge the MIT SuperCloud and Lincoln Laboratory Supercomputing Center for providing HPC resources that have contributed to the research results reported within this paper.

## References

- S. Graf and H. Luschgy, “Foundations of quantization for probability distributions”, Springer Science & Business Media, 2000.
- S. Lloyd, “Least squares quantization in PCM”, *IEEE transactions on information theory* **28** (1982), no. 2, 129–137.
- C. P. Robert, G. Casella, and G. Casella, “Monte Carlo statistical methods”, Springer, 1999.
- F. Bach, “On the equivalence between kernel quadrature rules and random feature expansions”, *The Journal of Machine Learning Research* **18** (2017), no. 1, 714–751, [arXiv:1502.06800](https://arxiv.org/abs/1502.06800).
- L. Chizat, E. Oyallon, and F. Bach, “On lazy training in differentiable programming”, *Advances in neural information processing systems* **32** (2019) [arXiv:1812.07956](https://arxiv.org/abs/1812.07956).
- M. Arbel, A. Korba, A. Salim, and A. Gretton, “Maximum mean discrepancy gradient flow”, *Advances in Neural Information Processing Systems* **32** (2019) [arXiv:1906.04370](https://arxiv.org/abs/1906.04370).

- K. Muandet, K. Fukumizu, B. Sriperumbudur, B. Schölkopf, *et al.*, “Kernel mean embedding of distributions: A review and beyond”, *Foundations and Trends® in Machine Learning* **10** (2017), no. 1-2, 1–141, [arXiv:1605.09522](#).
- J. Weed and F. Bach, “Sharp asymptotic and finite-sample rates of convergence of empirical measures in Wasserstein distance”, *Bernoulli* **25** (2019), no. 4A, 2620 – 2648, [arXiv:1707.00087](#).
- A. Gretton, K. Fukumizu, C. Teo, L. Song, B. Schölkopf, and A. Smola, “A kernel statistical test of independence”, *Advances in neural information processing systems* **20** (2007).
- A. Gretton, K. M. Borgwardt, M. J. Rasch, B. Schölkopf, and A. Smola, “A kernel two-sample test”, *The Journal of Machine Learning Research* **13** (2012), no. 1, 723–773.
- G. K. Dziugaite, D. M. Roy, and Z. Ghahramani, “Training generative neural networks via maximum mean discrepancy optimization”, *arXiv preprint*, 2015 [arXiv:1505.03906](#).
- C.-L. Li, W.-C. Chang, Y. Cheng, Y. Yang, and B. Póczos, “MMD GAN: Towards deeper understanding of moment matching network”, *Advances in neural information processing systems* **30** (2017) [arXiv:1705.08584](#).
- S. Chewi, J. Niles-Weed, and P. Rigollet, “Statistical optimal transport”, *arXiv preprint*, 2024 [arXiv:2407.18163](#).
- G. Peyré and M. Cuturi, “Computational optimal transport: With applications to data science”, *Foundations and Trends® in Machine Learning* **11** (2019), no. 5-6, 355–607, [arXiv:1803.00567](#).
- R. Jordan, D. Kinderlehrer, and F. Otto, “The variational formulation of the Fokker–Planck equation”, *SIAM journal on mathematical analysis* **29** (1998), no. 1, 1–17.
- F. Otto, “The geometry of dissipative evolution equations: the porous medium equation”, *Communications in Partial Differential Equations*, 2001.
- S. Kondratyev, L. Monsaingeon, and D. Vorotnikov, “A new optimal transport distance on the space of finite Radon measures”, *Advances in Differential Equations* **21** November (2016) [arXiv:1505.07746](#).
- K. Craig and A. Bertozzi, “A blob method for the aggregation equation”, *Mathematics of computation* **85** (2016), no. 300, 1681–1717, [arXiv:1405.6424](#).
- F. Santambrogio, “{Euclidean, metric, and Wasserstein} gradient flows: an overview”, *Bulletin of Mathematical Sciences* **7** (2017) 87–154, [arXiv:1609.03890](#).
- T. O. Gallouët and L. Monsaingeon, “A JKO splitting scheme for Kantorovich–Fisher–Rao gradient flows”, *SIAM Journal on Mathematical Analysis* **49** (2017), no. 2, 1100–1130, [arXiv:1602.04457](#).
- J. A. Carrillo, K. Craig, and F. S. Patacchini, “A blob method for diffusion”, *Calculus of Variations and Partial Differential Equations* **58** (2019) 1–53, [arXiv:1709.09195](#).
- S. Chewi, T. Le Gouic, C. Lu, T. Maunu, and P. Rigollet, “SVGD as a kernelized Wasserstein gradient flow of the chi-squared divergence”, *Advances in Neural Information Processing Systems* **33** (2020) 2098–2109, [arXiv:2006.02509](#).

- A. Salim, A. Korba, and G. Luise, “The Wasserstein proximal gradient algorithm”, *Advances in Neural Information Processing Systems* **33** (2020) 12356–12366, [arXiv:2002.03035](#).
- P. Glaser, M. Arbel, and A. Gretton, “KALE flow: A relaxed KL gradient flow for probabilities with disjoint support”, *Advances in Neural Information Processing Systems* **34** (2021) 8018–8031, [arXiv:2106.08929](#).
- A. Korba, P. Aubin-Frankowski, S. Majewski, and P. Ablin, “Kernel Stein discrepancy descent”, in “International Conference on Machine Learning”, pp. 5719–5730, PMLR. 2021. [arXiv:2105.09994](#).
- Y. Lu, D. Slepčev, and L. Wang, “Birth–death dynamics for sampling: global convergence, approximations and their asymptotics”, *Nonlinearity* **36** (2023), no. 11, 5731, [arXiv:2211.00450](#).
- A. Maurais and Y. Marzouk, “Sampling in unit time with kernel Fisher-Rao flow”, in “Proceedings of the 41st International Conference on Machine Learning”, vol. 235 of *Proceedings of Machine Learning Research*, pp. 35138–35162. PMLR, 21–27 Jul 2024. [arXiv:2401.03892](#).
- J.-J. Zhu and A. Mielke, “Kernel approximation of Fisher-Rao gradient flows”, *arXiv preprint*, 2024 [arXiv:2410.20622](#).
- E. Gladin, P. Dvurechensky, A. Mielke, and J.-J. Zhu, “Interaction-force transport gradient flows”, in “Advances in Neural Information Processing Systems”, A. Globerson, L. Mackey, D. Belgrave, A. Fan, U. Paquet, J. Tomczak, and C. Zhang, eds., vol. 37, pp. 14484–14508. Curran Associates, Inc., 2024. [arXiv:2405.17075](#).
- T. Karvonen and S. Särkkä, “Fully symmetric kernel quadrature”, *SIAM Journal on Scientific Computing* **40** (2018), no. 2, A697–A720, [arXiv:1703.06359](#).
- T. Karvonen and S. Särkkä, “Gaussian kernel quadrature at scaled Gauss–Hermite nodes”, *BIT Numerical Mathematics* **59** (2019), no. 4, 877–902, [arXiv:1803.09532](#).
- M. Ehler, M. Gräf, and C. J. Oates, “Optimal Monte Carlo integration on closed manifolds”, *Statistics and Computing* **29** (2019), no. 6, 1203–1214, [arXiv:1707.04723](#).
- A. Belhadji, R. Bardenet, and P. Chainais, “Kernel quadrature with DPPs”, *Advances in Neural Information Processing Systems* **32** (2019) [arXiv:1906.07832](#).
- A. Belhadji, R. Bardenet, and P. Chainais, “Kernel interpolation with continuous volume sampling”, *Proceedings of the 37th International Conference on Machine Learning*, 2020 725–735, [arXiv:2002.09677](#).
- A. Belhadji, “An analysis of Ermakov-Zolotukhin quadrature using kernels”, *Advances in Neural Information Processing Systems* **34** (2021) 27278–27289, [arXiv:2309.01200](#).
- T. Karvonen, S. Särkkä, and K. Tanaka, “Kernel-based interpolation at approximate Fekete points”, *Numerical Algorithms* **87** (2021) 445–468, [arXiv:1912.07316](#).
- E. Epperly and E. Moreno, “Kernel quadrature with randomly pivoted Cholesky”, *Advances in Neural Information Processing Systems* **36** (2023) 65850–65868, [arXiv:2306.03955](#).
- S. De M., “On optimal center locations for radial basis function interpolation: computational aspects”, *Rend. Splines Radial Basis Functions and Applications* **61** (2003), no. 3, 343–358.

- S. De M., R. Schaback, and H. Wendland, “Near-optimal data-independent point locations for radial basis function interpolation”, *Advances in Computational Mathematics* **23** (2005) 317–330.
- G. Santin and B. Haasdonk, “Convergence rate of the data-independent  $p$ -greedy algorithm in kernel-based approximation”, *arXiv preprint*, 2016 [arXiv:1612.02672](#).
- J. Oettershagen, “Construction of optimal cubature algorithms with applications to econometrics and uncertainty quantification”, Verlag Dr. Hut, 2017.
- F. Huszár and D. Duvenaud, “Optimally-weighted herding is Bayesian quadrature”, *arXiv preprint*, 2012 [arXiv:1204.1664](#).
- F.-X. Briol, C. Oates, M. Girolami, and M. A. Osborne, “Frank-Wolfe Bayesian quadrature: Probabilistic integration with theoretical guarantees”, *Advances in Neural Information Processing Systems* **28** (2015) [arXiv:1506.02681](#).
- S. Lacoste-Julien, F. Lindsten, and F. Bach, “Sequential kernel herding: Frank-Wolfe optimization for particle filtering”, in “Artificial Intelligence and Statistics”, pp. 544–552, PMLR. 2015. [arXiv:1501.02056](#).
- A. B. Owen, “Statistically efficient thinning of a Markov chain sampler”, *Journal of Computational and Graphical Statistics* **26** (2017), no. 3, 738–744, [arXiv:1510.07727](#).
- M. Riabiz, W. Y. Chen, J. Cockayne, P. Swietach, S. A. Niederer, L. Mackey, and C. J. Oates, “Optimal thinning of MCMC output”, *Journal of the Royal Statistical Society Series B: Statistical Methodology* **84** (2022), no. 4, 1059–1081, [arXiv:2005.03952](#).
- S. Hayakawa, H. Oberhauser, and T. Lyons, “Positively weighted kernel quadrature via subsampling”, *Advances in Neural Information Processing Systems* **35** (2022) 6886–6900, [arXiv:2107.09597](#).
- S. Hayakawa, H. Oberhauser, and T. Lyons, “Sampling-based Nyström approximation and kernel quadrature”, in “International Conference on Machine Learning”, pp. 12678–12699, PMLR. 2023.
- R. Dwivedi and L. Mackey, “Generalized kernel thinning”, *arXiv preprint*, 2021 [arXiv:2110.01593](#).
- R. Dwivedi and L. Mackey, “Kernel thinning”, *Journal of Machine Learning Research* **25** (2024), no. 152, 1–77, [arXiv:2105.05842](#).
- A. Chatalic, N. Schreuder, E. De Vito, and L. Rosasco, “Efficient numerical integration in reproducing kernel Hilbert spaces via leverage scores sampling”, *arXiv preprint*, 2023 [arXiv:2311.13548](#).
- Q. Du, V. Faber, and M. Gunzburger, “Centroidal Voronoi tessellations: Applications and algorithms”, *SIAM review* **41** (1999), no. 4, 637–676.
- M. Emelianenko, L. Ju, and A. Rand, “Nondegeneracy and weak global convergence of the Lloyd algorithm in  $\mathbb{R}^d$ ”, *SIAM Journal on Numerical Analysis* **46** (2008), no. 3, 1423–1441.
- J. Kieffer, “Exponential rate of convergence for Lloyd’s method I”, *IEEE Transactions on Information Theory* **28** (1982), no. 2, 205–210.
- X. Wu, “On convergence of Lloyd’s method I”, *IEEE Transactions on Information Theory* **38** (1992), no. 1, 171–174.

- Q. Du, M. Emelianenko, and L. Ju, “Convergence of the Lloyd algorithm for computing centroidal Voronoi tessellations”, *SIAM journal on numerical analysis* **44** (2006), no. 1, 102–119.
- G. Pagès and J. Yu, “Pointwise convergence of the Lloyd algorithm in higher dimension”, *SIAM Journal on Control and Optimization* **54** (2016), no. 5, 2354–2382, [arXiv:1401.0192](#).
- L. Portales, E. Cazelles, and E. Pauwels, “On the sequential convergence of Lloyd’s algorithms”, *arXiv preprint*, 2024 [arXiv:2405.20744](#).
- K. Fukunaga and L. Hostetler, “The estimation of the gradient of a density function, with applications in pattern recognition”, *IEEE Transactions on information theory* **21** (1975), no. 1, 32–40.
- M. A. Carreira-Perpinán, “A review of mean-shift algorithms for clustering”, *arXiv preprint*, 2015 [arXiv:1503.00687](#).
- D. Comaniciu and P. Meer, “Mean shift: A robust approach toward feature space analysis”, *IEEE Transactions on pattern analysis and machine intelligence* **24** (2002), no. 5, 603–619.
- Y. Cheng, “Mean shift, mode seeking, and clustering”, *IEEE transactions on pattern analysis and machine intelligence* **17** (1995), no. 8, 790–799.
- X. Li, Z. Hu, and F. Wu, “A note on the convergence of the mean shift”, *Pattern recognition* **40** (2007), no. 6, 1756–1762.
- M. A. Carreira-Perpinan, “Gaussian mean-shift is an EM algorithm”, *IEEE Transactions on Pattern Analysis and Machine Intelligence* **29** (2007), no. 5, 767–776.
- Y. A. Ghassabeh, “On the convergence of the mean shift algorithm in the one-dimensional space”, *Pattern Recognition Letters* **34** (2013), no. 12, 1423–1427, [arXiv:1407.2961](#).
- Y. A. Ghassabeh, “A sufficient condition for the convergence of the mean shift algorithm with Gaussian kernel”, *Journal of Multivariate Analysis* **135** (2015) 1–10.
- E. Arias-Castro, D. Mason, and B. Pelletier, “On the estimation of the gradient lines of a density and the consistency of the mean-shift algorithm”, *Journal of Machine Learning Research* **17** (2016), no. 206, 1–4.
- R. Yamasaki and T. Tanaka, “Properties of mean shift”, *IEEE transactions on pattern analysis and machine intelligence* **42** (2019), no. 9, 2273–2286.
- R. Yamasaki and T. Tanaka, “Convergence analysis of mean shift”, *IEEE Transactions on Pattern Analysis and Machine Intelligence*, 2024 [arXiv:2305.08463](#).
- L. Ambrosio, N. Gigli, and G. Savaré, “Gradient flows: in metric spaces and in the space of probability measures”, Springer Science & Business Media, 2008.
- L. Chizat, G. Peyré, B. Schmitzer, and F. Vialard, “An interpolating distance between optimal transport and Fisher–Rao metrics”, *Foundations of Computational Mathematics* **18** (2018) 1–44, [arXiv:1506.06430](#).
- M. Liero, A. Mielke, and G. Savaré, “Optimal entropy-transport problems and a new Hellinger–Kantorovich distance between positive measures”, *Inventiones mathematicae* **211** (2018), no. 3, 969–1117, [arXiv:1508.07941](#).

- Y. Lu, J. Lu, and J. Nolen, “Accelerating Langevin sampling with birth-death”, *arXiv preprint*, 2019 [arXiv:1905.09863](#).
- Y. Yan, K. Wang, and P. Rigollet, “Learning Gaussian mixtures using the Wasserstein–Fisher–Rao gradient flow”, *The Annals of Statistics* **52** (2024), no. 4, 1774–1795, [arXiv:2301.01766](#).
- C. T. Kelley, “Numerical methods for nonlinear equations”, *Acta Numerica* **27** (2018) 207–287.
- S. K. Lam, A. Pitrou, and S. Seibert, “Numba: A LLVM-based Python JIT compiler”, in “Proceedings of the Second Workshop on the LLVM Compiler Infrastructure in HPC”, pp. 1–6. 2015.
- A. Reuther, J. Kepner, C. Byun, S. Samsi, W. Arcand, D. Bestor, B. Bergeron, V. Gadepally, M. Houle, M. Hubbell, M. Jones, A. Klein, L. Milechin, J. Mullen, A. Prout, A. Rosa, C. Yee, and P. Michaleas, “Interactive supercomputing on 40,000 cores for machine learning and data analysis”, in “2018 IEEE High Performance extreme Computing Conference (HPEC)”, p. 1–6, IEEE. 2018.
- A. Pinkus, “n-Widths in Approximation Theory”, Springer Science & Business Media, 2012.
- J. Nocedal and S. Wright, “Numerical optimization”, Springer, 1999.
- G. Rotskoff, S. Jelassi, J. Bruna, and E. Vanden-Eijnden, “Global convergence of neuron birth-death dynamics”, in “International Conference on Machine Learning”. 2019. [arXiv:1902.01843](#).
- Y. De Castro and F. Gamboa, “Exact reconstruction using beurling minimal extrapolation”, *Journal of Mathematical Analysis and applications* **395** (2012), no. 1, 336–354, [arXiv:1103.4951](#).
- L. Chizat, “Sparse optimization on measures with over-parameterized gradient descent”, *Mathematical Programming* **194** (2022), no. 1, 487–532, [arXiv:1907.10300](#).
- A. Belhadji and R. Gribonval, “Sketch and shift: a robust decoder for compressive clustering”, *Transactions on Machine Learning Research*, 2024 [arXiv:2312.09940](#).

## A Additional numerical results

In this section, we provide details on the numerical simulations presented in Section 4, along with additional simulations.

### A.1 Implementation Details

- For WFR, we use a simple Runge-Kutta fourth order ODE solver for simulations. As this requires four evaluations of  $\mathbf{v}_0$  and  $\bar{\mathbf{v}}_1$  for each iteration, we only run the ODE for one fourth of the iterations compared to the other algorithms. Outside of the experiment setting, we suggest that common adaptive ODE solvers should provide better results. We also choose the diffusion rate  $\alpha$  according to naïve hyperparameter tuning, where simple experiments provide good results for about  $\alpha = 25$ .
- For MSIP, we use the damped fixed-point with  $\eta = 0.8$ . Moreover, we use standard floating-point methods to ensure stability when working with terms that take extremely small values such as the functions  $\mathbf{v}_0$  and  $\bar{\mathbf{v}}_1$ , which we employ for the squared exponential kernel.
- For MMDGF, we use a step-size of  $10^{-1}$  and inject noise at each iteration via  $\varepsilon_t \sim \mathcal{N}(0, \beta/\sqrt{t})$ , where  $t$  is the iteration and  $\beta = 0.05$ .
- For IFTFlow, we chose to implement the algorithm described in Gladin et al. (2024, Appendix A) with a regularization on the weight parameter of  $10^{-3}$  and, similar to the authors, performing the MMD geometry minimization via a single step of projected gradient descent.
- We observed that the methods proposed in both Arbel et al. (2019) and Gladin et al. (2024) resample the target distributions; however, we assume a fixed target distribution in each simulation and thus assume that the same  $N$  samples are available across all iterations of each algorithm.

### A.2 The generative model used in Section 4.1

We consider the following setting,  $\pi$  is the empirical measure associated to  $N = 1000$  i.i.d. samples from a mixture of Gaussians  $\sum_{m=1}^{\bar{M}} \pi_m \mathcal{N}(c_m, \Sigma_m)$ , where  $\bar{M} \in \mathbb{N}^*$  is the number of components of the mixture,  $c_1, \dots, c_{\bar{M}} \in \mathbb{R}^d$  are the means of the mixtures, and  $\Sigma_1, \dots, \Sigma_{\bar{M}} \in \mathbb{S}_d^{++}$  are the covariance matrices, and  $\pi_1, \dots, \pi_{\bar{M}}$  are the positive weights of the mixture which satisfy  $\sum_{m=1}^{\bar{M}} \pi_m = 1$ . For  $d = 2$  we take  $\bar{M} = 3$ , and for  $d = 100$  we take  $\bar{M} = 5$ . Figure 4 illustrates some marginals of the 100-dimensional distribution used in Section 4.1. The 100-dimensional distribution is marginally normalized to have covariance with ones on the diagonal.

### A.3 Additional results for the MNIST Simulation

#### A.3.1 The effect of additional iterations

Figure 5 shows the results of the simulation detailed in Section 4.2 after 15000 iterations for MSIP, WFR, Lloyd’s algorithm, and IFTFlow. We observe that their recovered images are less blurry compared to the results after 5000 iterations. Interestingly, one particle in the IFTFlow simulation reaches the support (and seems to visually correspond with the mode that IIDMS finds in Figure 3).

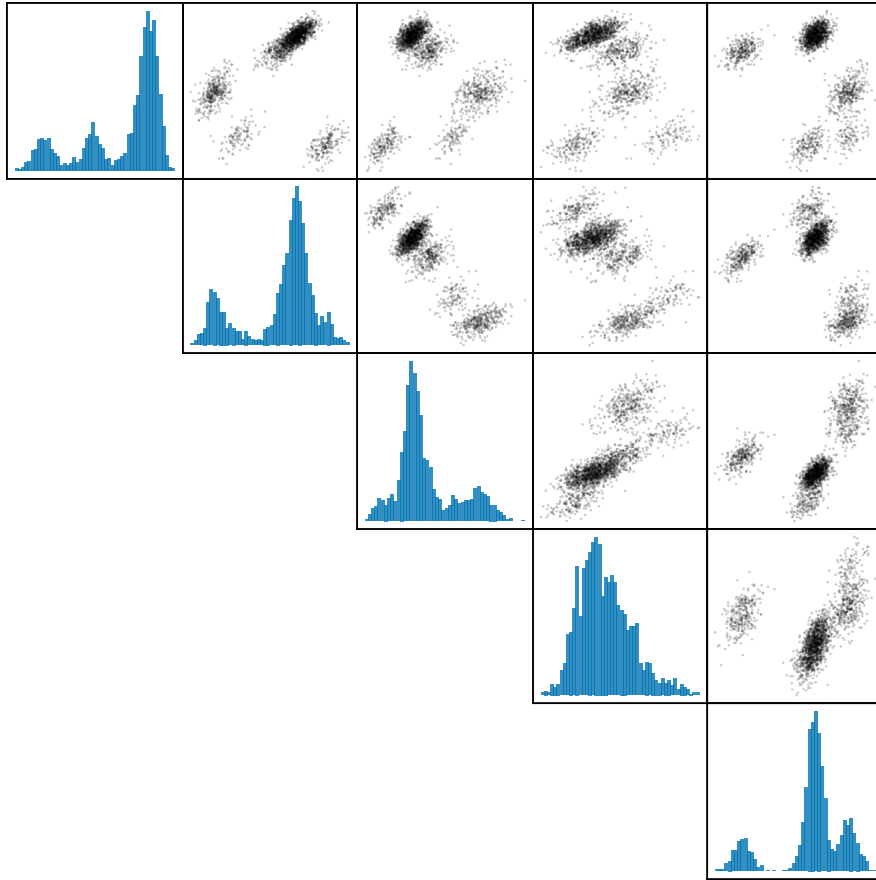


Figure 4: First five marginals of the 100-dimensional distribution used in Section 4.1

### A.3.2 Quantitative results for MNIST

In Figure 6, we calculate the MMD for each algorithm using the Matérn kernel with  $\sigma = 2.25$  and  $\nu = 1.5$ . We use 10 different initializations for the experiment and show the marginal median MMD at each iteration. Despite the fact that DMGD starts from a low level, the value of the MMD does not decrease over time for this algorithm. MSIP and WFR are the only two algorithms that enjoy substantial dynamics in these simulations, shown by their decay over time.

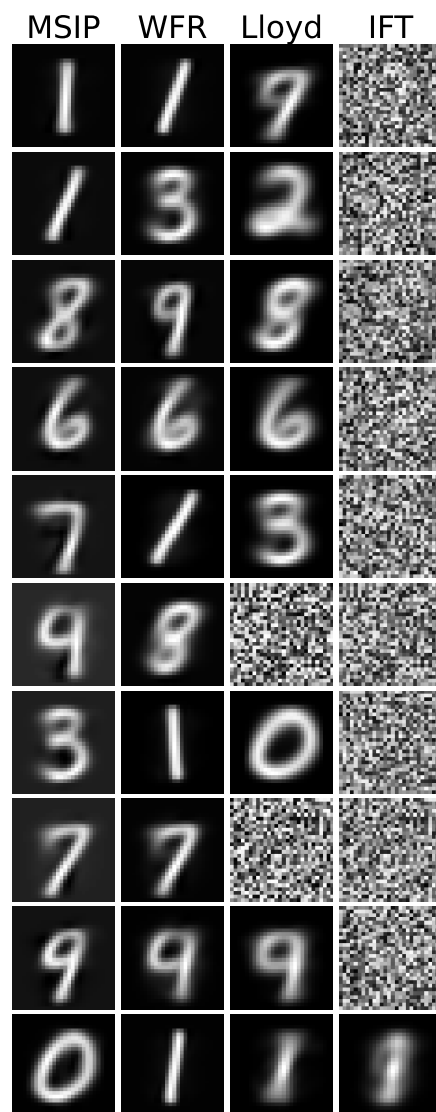


Figure 5: Comparison of four algorithms on MNIST for the iteration  $T = 15000$ .

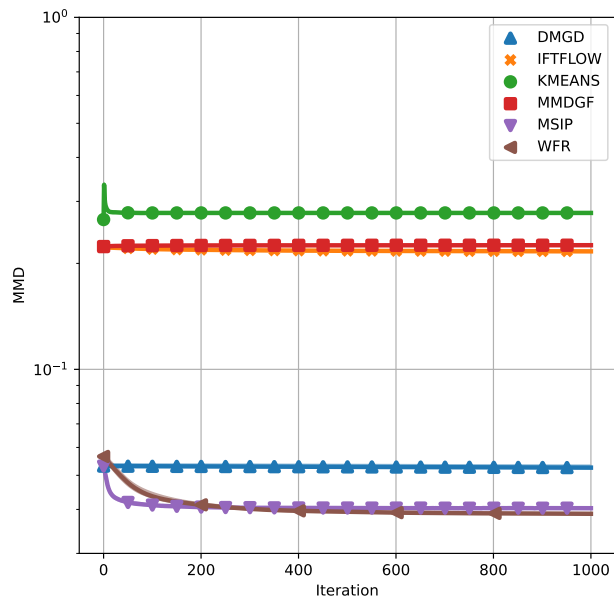


Figure 6: Comparison of different algorithms on MNIST for the iteration  $T = 1000$ .

## B Proofs

### B.1 Proof of Theorem 3.1

This is a ready extension to common proof techniques in, e.g., (Yan et al., 2024) and (Chewi et al., 2024, Section 5.7.). Let  $\varphi \in C_c^\infty$  be a test function. We have

$$\begin{aligned}
\frac{d}{dt} \int_{\mathbb{R}^d} \varphi(x) \mu_t(dx) &= \frac{d}{dt} \left[ \sum_{i=1}^M w_i^{(t)} \varphi(y_i^{(t)}) \right] \\
&= \sum_{i=1}^M \frac{d}{dt} w_i^{(t)} \varphi(y_i^{(t)}) + \sum_{i=1}^M w_i^{(t)} \frac{d}{dt} \varphi(y_i^{(t)}) \\
&= \sum_{i=1}^M \frac{d}{dt} w_i^{(t)} \varphi(y_i^{(t)}) + \sum_{i=1}^M w_i^{(t)} \langle \nabla \varphi(y_i^{(t)}), \frac{d}{dt} y_i^{(t)} \rangle \\
&= - \sum_{i=1}^M \tilde{\mathcal{F}}[\mu_t](y_i^{(t)}) w_i^{(t)} \varphi(y_i^{(t)}) - \alpha \sum_{i=1}^M w_i^{(t)} \langle \nabla \varphi(y_i^{(t)}), \nabla \tilde{\mathcal{F}}[\mu_t](y_i^{(t)}) \rangle \\
&= - \int_{\mathbb{R}^d} \tilde{\mathcal{F}}[\mu_t](x) \varphi(x) \mu_t(dx) - \alpha \int_{\mathbb{R}^d} \langle \nabla \varphi(x), \nabla \tilde{\mathcal{F}}[\mu_t](x) \rangle \mu_t(dx) \\
&= - \int_{\mathbb{R}^d} \varphi(x) \tilde{\mathcal{F}}[\mu_t](x) \mu_t(dx) + \alpha \int_{\mathbb{R}^d} \varphi(x) \operatorname{div}(\mu_t \nabla \tilde{\mathcal{F}}[\mu_t])(x) dx.
\end{aligned}$$

In other words,  $(\mu_t)_{t \geq 0}$  satisfies (20) in the sense of distributions.

### B.2 Proof of Theorem 3.2

Under Theorem 2.1, the equation (23) writes for  $j \in [M]$

$$\sum_{i=1}^M w_i y_i \bar{\kappa}(y_i, y_j) = \left( \sum_{i=1}^M w_i \bar{\kappa}(y_i, y_j) - \int_{\mathcal{X}} \bar{\kappa}(x, y_j) d\pi(x) \right) y_j + \int_{\mathcal{X}} x \bar{\kappa}(x, y_j) d\pi(x), \quad (36)$$

which can be expressed in matrix form as (24).

### B.3 Proof of Theorem 3.3

First, let  $C_\pi := \int_{\mathcal{X}} \int_{\mathcal{X}} \kappa(x, x') d\pi(x) d\pi(x')$ . Then, observe that for  $Y \in \mathcal{X}_\neq^M$  we have

$$F_M(Y) = \frac{1}{2} \left( C_\pi + 2 \langle \hat{\mathbf{w}}(Y), \mathbf{v}_0(Y) \rangle + \langle \hat{\mathbf{w}}(Y), \mathbf{K}(Y) \hat{\mathbf{w}}(Y) \rangle \right), \quad (37)$$

where  $\hat{\mathbf{w}}(Y)$  is defined by (4) respectively, and  $\mathbf{v}_0$  is given by (5).

Now, using (4), we prove that

$$\langle \hat{\mathbf{w}}(Y), \mathbf{v}_0(Y) \rangle = \langle \mathbf{v}_0(Y), \mathbf{K}(Y)^{-1} \mathbf{v}_0(Y) \rangle = \langle \hat{\mathbf{w}}(Y), \mathbf{K}(Y) \hat{\mathbf{w}}(Y) \rangle. \quad (38)$$

In particular, the expression of  $F_M(Y)$  simplifies further to

$$F_M(Y) = \frac{1}{2} \left( C_\pi - \langle \hat{\mathbf{w}}(Y), \mathbf{v}_0(Y) \rangle \right) = \frac{1}{2} \left( C_\pi - \langle \hat{\mathbf{w}}(Y), \mathbf{K}(Y) \hat{\mathbf{w}}(Y) \rangle \right).$$

In the following, we proceed to the calculation of the gradient of  $F_M$ . First, for a configuration  $Y \in \mathcal{X}^M$ , we define  $y_{ij}$  as the scalar in the  $j$ th dimension of node  $y_i$ . Now, we seek the gradient  $\nabla F_M \in \mathbb{R}^{M \times d}$ . In particular, for  $i \in [M]$  and  $j \in [d]$ , we use  $\nabla_{ij} F_M(Y)$  to denote the  $(i, j)$  entry of  $\nabla F_M(Y)$  corresponding to input  $y_{ij}$  evaluated at  $Y \in \mathbb{R}^{M \times d}$ . Moreover, we define  $\nabla_{ij} \mathbf{K}(Y) \in \mathbb{R}^{M \times M}$  to be the differentiation of each element of matrix  $\mathbf{K}(Y)$  with respect to the  $j$ th coordinate of vector  $y_i$ . Similarly, for kernel mean embedding  $\mathbf{v}_0 : \mathcal{X}_{\neq}^M \rightarrow \mathbb{R}^M$  we denote by  $\nabla_{ij} \mathbf{v}_0$  the vector obtained by differentiating each element of  $\mathbf{v}_0$  with respect to the  $j$ th coordinate of vector  $y_i$ . In other words, we have

$$\nabla_{ij} F_M = \frac{\partial}{\partial y_{ij}} F_M(Y), \quad \nabla_{ij} \mathbf{K}(Y) = \frac{\partial}{\partial y_{ij}} \mathbf{K}(Y), \quad \nabla_{ij} \mathbf{v}(Y) = \frac{\partial}{\partial y_{ij}} \mathbf{v}(Y) \quad (39)$$

Using (38) and matrix calculus, we have

$$2\nabla_{ij} F_M(Y) = 2\langle \hat{\mathbf{w}}(Y), \mathbf{K}(Y) \nabla_{ij} \hat{\mathbf{w}}(Y) \rangle + \langle \hat{\mathbf{w}}(Y), \nabla_{ij} \mathbf{K}(Y) \hat{\mathbf{w}}(Y) \rangle. \quad (40)$$

Since  $\hat{\mathbf{w}}(Y) = \mathbf{K}(Y)^{-1} \mathbf{v}_0(Y)$ , we get

$$\nabla_{ij} \hat{\mathbf{w}}(Y) = \mathbf{K}(Y)^{-1} \nabla_{ij} \mathbf{v}_0(Y) - \mathbf{K}(Y)^{-1} \nabla_{ij} \mathbf{K}(Y) \mathbf{K}(Y)^{-1} \mathbf{v}_0(Y), \quad (41)$$

$$\mathbf{K}(Y) \nabla_{ij} \hat{\mathbf{w}}(Y) = \nabla_{ij} \mathbf{v}_0(Y) - \nabla_{ij} \mathbf{K}(Y) \hat{\mathbf{w}}(Y) \quad (42)$$

so that

$$\langle \hat{\mathbf{w}}(Y), \mathbf{K}(Y) \nabla_{ij} \hat{\mathbf{w}}(Y) \rangle = \langle \hat{\mathbf{w}}(Y), \nabla_{ij} \mathbf{v}_0(Y) \rangle - \langle \hat{\mathbf{w}}(Y), (\nabla_{ij} \mathbf{K}(Y)) \hat{\mathbf{w}}(Y) \rangle. \quad (43)$$

Therefore, we have

$$\begin{aligned} 2\nabla_{ij} F_M(Y) &= \langle \hat{\mathbf{w}}(Y), (\nabla_{ij} \mathbf{K}(Y)) \hat{\mathbf{w}}(Y) \rangle + \\ &\quad + 2(\langle \hat{\mathbf{w}}(Y), \nabla_{ij} \mathbf{v}_0(Y) \rangle - \langle \hat{\mathbf{w}}(Y), (\nabla_{ij} \mathbf{K}(Y)) \hat{\mathbf{w}}(Y) \rangle) \\ &= 2\langle \hat{\mathbf{w}}(Y), \nabla_{ij} \mathbf{v}_0(Y) \rangle - \langle \hat{\mathbf{w}}(Y), (\nabla_{ij} \mathbf{K}(Y)) \hat{\mathbf{w}}(Y) \rangle. \end{aligned} \quad (44)$$

Now recall that

$$[\nabla_{ij} \mathbf{K}(Y)]_{m_1, m_2} = \nabla_{ij} \kappa(y_{m_1}, y_{m_2}),$$

for all  $m_1, m_2 \in [M]$ . Therefore, under Theorem 2.1,

$$\nabla_{ij} \kappa(y_{m_1}, y_{m_2}) = \delta_{i, m_1} (y_{m_2 j} - y_{ij}) \bar{\kappa}(y_i, y_{m_2}) + \delta_{i, m_2} (y_{m_1 j} - y_{ij}) \bar{\kappa}(y_{m_1}, y_i). \quad (45)$$

First, we denote  $[\mathbf{a} \otimes \mathbf{b}]_{ij} = a_i b_j$  as the outer product between vectors  $\mathbf{a}$  and  $\mathbf{b}$  with possibly different dimensions. We also denote  $\mathbf{a} \odot \mathbf{b}$  as the elementwise (i.e., Hadamard) product between  $\mathbf{a}$  and  $\mathbf{b}$  with identical dimensions. Then, we have

$$\nabla_{ij} \mathbf{K}(Y) = \mathbf{b}_{ij} \otimes \mathbf{e}_i + \mathbf{e}_i \otimes \mathbf{b}_{ij},$$

where  $\mathbf{e}_i$  is the  $i$ th elementary vector, i.e.,  $[\mathbf{e}_i]_m = \delta_{im}$ , and we define

$$\mathbf{b}_{ij} := (Y_j - y_{ij} \mathbf{1}) \odot \bar{\mathbf{K}}_i = Y_j \odot \bar{\mathbf{K}}_i - y_{ij} \bar{\mathbf{K}}_i,$$

with  $Y_j \in \mathbb{R}^M$  is the vector containing the  $j$ -th entry of each  $y_i$ , identical to the  $j$ th column of the matrix  $Y$ , and  $\bar{\mathbf{K}}_i = \bar{\mathbf{K}}(Y) \mathbf{e}_i$ . Then,

$$\begin{aligned} \langle \hat{\mathbf{w}}(Y), (\nabla_{ij} \mathbf{K}(Y)) \hat{\mathbf{w}}(Y) \rangle &= \langle \hat{\mathbf{w}}(Y), (\mathbf{b}_{ij} \otimes \mathbf{e}_i + \mathbf{e}_i \otimes \mathbf{b}_{ij}) \hat{\mathbf{w}}(Y) \rangle \\ &= 2\hat{w}_i(Y) \langle \hat{\mathbf{w}}(Y), \mathbf{b}_{ij} \rangle \\ &= 2\hat{w}_i(Y) \left( \langle \hat{\mathbf{w}}(Y), Y_j \odot \bar{\mathbf{K}}_i - y_{ij} \bar{\mathbf{K}}_i \rangle \right) \\ &= 2\hat{w}_i(Y) \left( \langle \hat{\mathbf{w}}(Y), Y_j \odot \bar{\mathbf{K}}_i \rangle - y_{ij} \langle \hat{\mathbf{w}}(Y), \bar{\mathbf{K}}_i \rangle \right) \end{aligned} \quad (46)$$

For  $m \in [M]$ , we recall that  $\nabla\kappa$  is bounded on  $\mathcal{X} \times \mathcal{X}$  to find

$$\begin{aligned}\nabla_{ij}\mathbf{v}_0(Y) &= (\nabla_{ij}v_0(y_i)) \mathbf{e}_i \\ \nabla_{ij}v_0(y_i) &= \int_{\mathcal{X}} \nabla_{ij}\kappa(x, y_i) \, d\pi(x) \\ &= \int_{\mathcal{X}} (x_j - y_{ij}) \bar{\kappa}(x, y_i) \, d\pi(x) \\ &= \int_{\mathcal{X}} x_j \bar{\kappa}(x, y_i) \, d\pi(x) - y_{ij} \bar{v}_0(y_i),\end{aligned}$$

where  $x_j \in \mathbb{R}$  is the  $j$ th entry of integration variable  $x \in \mathbb{R}^d$ , and we recall that  $\bar{v}_0(y) = \int_{\mathcal{X}} \bar{\kappa}(x, y) \, d\pi(x)$ . We then have

$$\nabla_{ij}\mathbf{v}_0(Y) = ([\bar{v}_1(y_i)]_j - y_{ij} \bar{v}_0(y_i)) \mathbf{e}_i.$$

Thus,

$$\langle \hat{\mathbf{w}}(Y), \nabla_{ij}\mathbf{v}_0(Y) \rangle = \hat{w}_i(Y) ([\bar{v}_1(y_i)]_j - y_{ij} \bar{v}_0(y_i)). \quad (47)$$

Combining (44), (46) and (47), we obtain

$$\begin{aligned}2\nabla_{ij}F_M(Y) &= -2\hat{w}_i(Y) ([\bar{v}_1(y_i)]_j - y_{ij} \bar{v}_0(y_i) - \langle \hat{\mathbf{w}}(Y), Y_j \odot \bar{\mathbf{K}}_i \rangle + y_{ij} \langle \hat{\mathbf{w}}(Y), \bar{\mathbf{K}}_i \rangle) \\ &= -2\hat{w}_i(Y) ([\bar{v}_1(y_i)]_j - y_{ij} \bar{v}_0(y_i) + y_{ij} \langle \hat{\mathbf{w}}(Y), \bar{\mathbf{K}}_i \rangle - \langle \hat{\mathbf{w}}(Y), Y_j \odot \bar{\mathbf{K}}_i \rangle)\end{aligned} \quad (48)$$

Now,

$$\begin{aligned}-y_{ij} \bar{v}_0(y_i) + y_{ij} \langle \hat{\mathbf{w}}(Y), \bar{\mathbf{K}}_i \rangle &= y_{ij} \left( \sum_{m=1}^M \hat{w}_m(Y) \bar{\kappa}(y_i, y_m) - \int_{\mathcal{X}} \bar{\kappa}(x, y_i) \, d\pi(x) \right) \\ &= [\bar{\mathbf{u}}(Y)]_i\end{aligned} \quad (49)$$

which matches the definition of  $\bar{\mathbf{u}}(Y)$  in Equation (25). By the symmetry of  $\bar{\kappa}$ ,

$$\begin{aligned}\langle \hat{\mathbf{w}}(Y), Y_j \odot \bar{\mathbf{K}}_i \rangle &= \sum_{m=1}^M \hat{w}_m(Y) y_{mj} \bar{\kappa}(y_m, y_i) \\ &= \sum_{m=1}^M \bar{\kappa}(y_i, y_m) \hat{w}_m(Y) y_{mj} \\ &= \langle \mathbf{e}_i, \bar{\mathbf{K}}(Y) \mathbf{W}(Y) Y_j \rangle \\ &= [\bar{\mathbf{K}}(Y) \mathbf{W}(Y) Y]_{i,j}\end{aligned} \quad (50)$$

where  $\mathbf{W}(Y) \in \mathbb{R}^{M \times M}$  satisfies  $[\mathbf{W}(Y)]_{i,m} = \hat{w}_i(Y) \delta_{i,m}$ . Combining (49), (50), and the fact that  $[\bar{v}_1(y_i)]_j$  is the  $(i, j)$ -th entry of the matrix  $\bar{\mathbf{v}}_1(Y)$ , we conclude that

$$([\bar{v}_1(y_i)]_j - y_{ij} \bar{v}_0(y_i) + y_{ij} \langle \hat{\mathbf{w}}(Y), \bar{\mathbf{K}}_i \rangle - \langle \hat{\mathbf{w}}(Y), Y_j \odot \bar{\mathbf{K}}_i \rangle)$$

is the  $(i, j)$ -entry of the matrix  $\bar{\mathbf{v}}_1(Y) + \bar{\mathbf{u}}(Y) - \bar{\mathbf{K}}(Y) \mathbf{W}(Y) Y$ . Thus, (48) is the  $(i, j)$ -entry of the matrix

$$2\mathbf{W}(Y) (\bar{\mathbf{K}}(Y) \mathbf{W}(Y) Y - \bar{\mathbf{v}}_1(Y) - \bar{\mathbf{u}}(Y)). \quad (51)$$

In other words,

$$\begin{aligned}\nabla F_M(Y) &= \mathbf{W}(Y) (\bar{\mathbf{K}}(Y) \mathbf{W}(Y) Y - \bar{v}_1(Y) - \bar{u}(Y)) \\ &= \mathbf{W}(Y) (\bar{\mathbf{K}}(Y) \mathbf{W}(Y) Y - \hat{v}_1(Y)),\end{aligned}\tag{52}$$

where  $\hat{v}_1(Y) = \bar{v}_1(Y) + \bar{u}(Y)$  as in (27). When the matrices  $\mathbf{W}(Y)$  and  $\bar{\mathbf{K}}(Y)$  are non-singular, we have

$$\nabla F_M(Y) = \mathbf{W}(Y) \bar{\mathbf{K}}(Y) \mathbf{W}(Y) (Y - \mathbf{W}(Y)^{-1} \bar{\mathbf{K}}(Y)^{-1} \hat{v}_1(Y)).\tag{53}$$

Finally, observe that the function  $\Psi_{\text{MSIP}}$  defined by (28) satisfies

$$\Psi_{\text{MSIP}}(Y) = \mathbf{W}(Y)^{-1} \bar{\mathbf{K}}(Y)^{-1} \hat{v}_1(Y).\tag{54}$$

#### B.4 Proof of Theorem 3.4

We again define  $C_\pi = \int_{\mathcal{X}} \int_{\mathcal{X}} \kappa(x, x') d\pi(x) d\pi(x')$ . First, for  $w \in \mathbb{R}$  and  $y \in \mathcal{X}$ , we have

$$\mathcal{F}(w\delta_y) = \frac{1}{2} (C_\pi - 2wv_0(y) + w^2\kappa(y, y)).\tag{55}$$

Since this is a quadratic form on  $w$ , we get

$$\arg \min_{w \in \mathbb{R}} \mathcal{F}(w\delta_y) = \frac{v_0(y)}{\kappa(y, y)}.\tag{56}$$

Thus, by (31) in Theorem 3.3, we get

$$\nabla F_1(y) = \frac{v_0(y)}{\kappa(y, y)} \left( \bar{\kappa}(y, y) \frac{v_0(y)}{\kappa(y, y)} y - \bar{u}(y) - \bar{v}_1(y) \right).\tag{57}$$

By definition (25), we have

$$\bar{u}(y) = \left( \frac{v_0(y)}{\kappa(y, y)} \bar{\kappa}(y, y) - \bar{v}_0(y) \right) y.\tag{58}$$

By rearranging (58), we see

$$\frac{v_0(y)}{\kappa(y, y)} \bar{\kappa}(y, y) y - \bar{u}(y) = \bar{v}_0(y) y.\tag{59}$$

Combining (57) and (59)

$$\nabla F_1(y) = \frac{v_0(y)}{\kappa(y, y)} \left( \bar{v}_0(y) y - \bar{v}_1(y) \right).\tag{60}$$